A Study of the Effect of Nanosized Particles on Transient Liquid Phase Diffusion Bonding Al6061 Metal–Matrix Composite (MMC) Using Ni/Al_2O_3 Nanocomposite Interlayer

KAVIAN O. COOKE

Transient liquid phase (TLP) diffusion bonding of Al-6061 containing 15 vol pct alumina particles was carried out at 873 K (600 °C) using electrodeposited nanocomposite coatings as the interlayer. Joint formation was attributed to the solid-state diffusion of Ni into the Al-6061 alloy followed by eutectic formation and isothermal solidification of the joint region. An examination of the joint region using an electron probe microanalyzer (EPMA), transmission electron microscopy (TEM), wavelength-dispersive spectroscopy (WDS), and X-ray diffraction (XRD) showed the formation of intermetallic phases such as Al_3Ni, Al_9FeNi, and Ni_3Si within the joint zone. The result indicated that the incorporation of 50 nm Al_2O_3 dispersions into the interlayer can be used to improve the joint significantly.

DOI: 10.1007/s11663-012-9643-5

I. INTRODUCTION

TRANSIENT liquid phase (TLP) diffusion bonding has been studied extensively for joining particle reinforced Al-metal–matrix composites (MMCs) as a means of improving joint shear strength.[1–3] The process depends on the formation of a thin, continuous layer of liquid at the joint interface, through a eutectic or peritectic reaction between the interlayer and the base metal. This reaction also has the advantage of being able to remove surface oxides, thereby allowing the liquid film to wet the contacting metallic substrates. By holding the sample at the bonding temperature, the liquid phase solidifies isothermally, followed by homogenization of the joint region.[4–6] The scientific literature shows that the composition of the interlayer can affect significantly the quality of the joints produced.[3–6] When monolithic interlayers are used to join particle-reinforced Al-MMCs, the formation of dispersion-free zones in the joint center has been reported.[6,8] However, it has been shown in the literature that the joint region can be reinforced by two methods, both of which involves the incorporation of strengthening particles in the bond region, either by using a particle-reinforced filler material or by the melt back.[4,7,8]

In recent studies, it has been shown that Sn-based interlayers reinforced with SiC can improve the joint strength of Al6061 + 25 pct (Al_2O_3)p by approximately 100 pct when compared with unreinforced Sn-based joints formed by ultrasonic assisted soldering.[9–11] However, the joint formed normally has a strength far lower than that of the parent metal, which limits the use of the components made by this method to less critical applications. Yan *et al.*[12] developed a SiC particle-reinforced, Zn-based filler that was used to join the SiCp/A356 composite. The results indicated that with the used of ultrasonic vibration, suitable particle distribution and reduced void formation were achieved. Cooke *et al.*[13–15] used a Ni/Al_2O_3 nanocomposite interlayer to join Al-6061/15 vol pct Al_2O_3. The results showed that the TLP bonds reinforced with nanosized Al_2O_3 particles had the potential of increasing the bond strength significantly. Although numerous studies have focused on exploring the use of particle-reinforced fillers in joining, the mechanism of strengthening has not been reported.

The current study investigates the effects of particle size on the microstructural development across the joint region and subsequent effect on joint shear strength. The mechanisms of joint strengthening and joint failure during shear testing were also studied.

II. MATERIAL AND METHODS

A. *Materials*

In this study, an Al-6061 alloy containing 15 vol pct of alumina (Al_2O_3) particles with an average size of 28 μm was used. The microstructure and composition of the material is shown in Figure 1 and Table I, respectively.[13–15]

B. *Sample Preparation and Bonding Process*

As described previously,[13–15] the specimens were prepared for bonding by cutting to a dimension of 10 × 10 × 5 mm. A hole was drilled to a depth of 3 mm at 1 mm from the bonding interface. The bonding surfaces were prepared to 800-grit SiC finish and subsequently polished to 1 μm using a diamond suspension and then cleaned in an acetone bath.

KAVIAN O. COOKE, Lecturer, is with the Department of Mechanical Engineering, University of Technology, Kingston 6, Jamaica. Contact e-mail: Kavian_cooke@yahoo.com
Manuscript submitted December 29, 2011.
Article published online March 3, 2012.

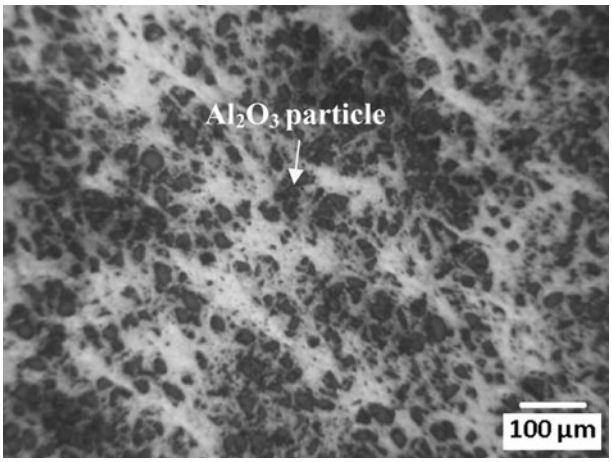

Fig. 1—Microstructure of the Al-6061/15 vol pct Al_2O_3p metal–matrix composite.

Table I. Composition of Al6061/15 vol pct Al_2O_3p MMC

Composition wt pct								
Fe	Cu	Mg	Mn	Cr	Ti	Zn	Si	Al
0.03	0.11	1.09	0.05	0.08	0.09	0.15	0.69	bal

Prior to bonding, one piece of each couple was electroplated with a 5-μm-thick Ni-coatings codeposited with Al_2O_3 particles of sized 50 and 500 nm (separate coating solution prepared for each particle size). A comparative analysis between the nano-Al_2O_3 reinforced TLP joints and the pure Ni joints were presented previously.[13] Therefore, the current study evaluates the effect of interlayer particle size on the joint strength. The electrodeposition of Ni onto the Al-6061 surfaces was carried out in a 250-mL glass beaker using a James Watt nickel bath recipe.[16] For the codeposition process, 50 g/L of Al_2O_3 was added to the nickel bath and kept in suspension by a magnetic stirrer. The specimens were assembled at room temperature and placed on the lower platen within the induction coil. An ungrounded k-type thermocouple was inserted into the hole located approximately 1 mm from the joint interface. Once a vacuum of 4×10^{-4} torr (0.053 Pa) was achieved, the assembly was heated to a bonding temperature of 873 K (600 °C). This temperature was selected to be above the Al-Ni-Si ternary eutectic temperature of 838 K (565 °C).[17]

The specimens were brought to the joining temperature at a heating rate of 65 °C/min and then held at that temperature for 10 minutes. The power was turned off and the specimen was cooled to room temperature in vacuum once the bonding process was completed. The bonded specimens were sectioned perpendicular to the bond line by an abrasive saw and mounted in Bakelite. The mounted specimens were prepared according to ASTM B 253.[18] The samples were ground progressively on silicon carbide papers from 240 to 800 grit, followed by a final polish to 1-μm finish. A mixture containing 2 mL HF, 3 mL HCL, 5 mL HNO_3, and 190 mL H_2O was used as the etchant to reveal the aluminum grain structure.

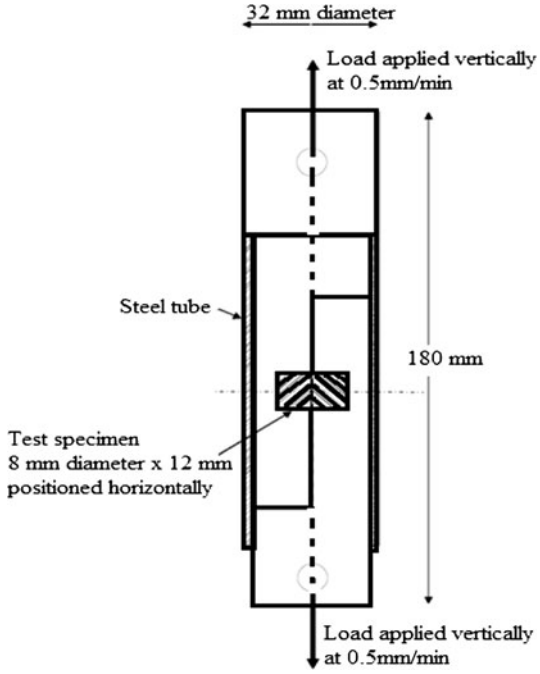

Fig. 2—Schematic of shear test apparatus.[18]

The bonded samples were machined to 8 mm diameter to eliminate edge effects. Bonded specimens of approximately 10 mm length and 8 mm diameter were loaded into a specially prepared apparatus, which is shown schematically in Figure 2. The grips of this apparatus were pulled in tension by a Tinius-Olsen tensile testing machine at a cross-head speed of 0.5 mm/min in the position control mode, such that the specimen experienced pure shear stress across the bond interface. The shear strength was calculated by dividing the maximum load by the bonded area. For each bonding condition, three specimens were tested and the average value was used to determine the joint shear strength (bond strength).

Examinations of the joints were performed using an optical microscope an electron probe microanalyzer (EPMA) and a transmission electron microscope (TEM). Quantitative compositional analyses were carried out using wavelength-dispersive spectroscopy (WDS), and X-ray diffraction (XRD). Microhardness testing was performed on the cross section of the joints according to ASTM E92 standard test method for Vickers microhardness testing. Indentations were made at 100 μm spacing using a diamond tip indenter to which a 0.2-kg load was applied for 15 seconds, after which the length of the diagonals was measured and the hardness number was recorded from the tables.

For TEM analyses, sections of the bonded region were cut to $6 \times 5 \times 1.5$ mm using a thin, diamond-tip cutter and subsequently mechanically grounded using 600-grit abrasive paper to a thickness of approximately 200 μm. A disk of 3 mm diameter was punched from the 200-μm foil and subsequently grinded mechanically to

25 μm. The grinded samples were thinned by the electropolishing method. This was done in a solution containing 150 g/L Na_2CO_3 + 50 g/L Na_3PO_4 + 30 g/L. The solution was maintained at a temperature of 313 K (40 °C) and a voltage of 20 V. All the thinned foils were examined with a JEOL TEM 2000FX (JEOL Ltd., Tokyo, Japan) TEM at an accelerating voltage of 200 kV.

III. RESULTS AND DISCUSSION

A. *Ni-Al_2O_3 Coating*

The Ni/Al_2O_3p coating thickness was controlled by the current density and deposition time. The actual amount of Ni/Al_2O_3p electroplated onto a surface was determined by the weight gained by the sample during the plating process. Figure 3(a) shows a scanning electron microscopy (SEM) micrograph of the coating produced by coelectrodeposition of Ni and nanosized Al_2O_3 particles. A point counting analysis using ImageJ software (National Institutes of Health, Bethesda, MD) indicated that of approximately 18 vol pct nano-Al_2O_3 particles were present in the coating. This finding was also confirmed by digital X-ray mapping shown in Figure 4.

The density of the composite coating can be evaluated using Eq. [1], where $x_{v_3} = 18$ pct is the volume fraction of alumina particles in the coating. $\rho_{Al_2O_3}$ and ρ_{Ni} are the density of the ceramic powder and the nickel matrix, respectively.

$$\rho_C = \rho_{Al_2O_3} x_{v_3} + \rho_{Ni} (1 - x_{v_3}) \quad [1]$$

The coating thickness was calculated using Eq. [1]:

$$\rho_C = \frac{\text{mass of coating}}{\text{area} \times \text{thickness}} = \frac{m}{A \times t} \quad [2]$$

where ρ_C is the density of the composite coating, A is the cross-sectional area, t is the coating thickness, and m is the mass gained during the plating process. By assuming that $\rho_{Al_2O_3} = 3.87$ g/cm^3 and $\rho_{Ni} = 8.91$ g/cm^3. The density of the composite coating was found to be 8.09 g/cm^3. The thickness of the coatings was obtained by manipulating the deposition time. The results indicate that for a coating thickness of 5 μm, a deposition time of 15 minutes was required.

SEM analyses of the coating revealed the absence of surface defects and interfacial voids; however, Al_2O_3 particle clusters were present in the coating. The particle clustering is believed to have occurred in the powder prior to the coating process as indicated by the TEM micrograph of the as-received Al_2O_3 powder shown in Figure 3(b).

B. *Microstructure of the Joint*

In this study, diffusion bonding was carried out at a temperature of 873 K (600 °C). The effect of nanosized particles on the microstructural development across the joint region and the subsequent effects on mechanical properties such as shear strength and microhardness were studied. Figure 5 shows the microstructure of a joint bonded using a 5-μm-thick Ni coating dispersed with 50-nm Al_2O_3 particles. From the micrograph, a 50-μm-wide particle segregated zone was observed within the joint center. Also present at the center of the joint are dark clumps, which an EDS analysis suggested are oxide particles (Figures 5(a) and (b)). The observed oxide clusters are likely to be Al_2O_3 particles that agglomerated during the deposition process. When the coating particle size was increased to 500 nm Al_2O_3, a similar result was obtained (Figure 5(b)). Additionally, a thin, segregated zone was formed at the joint center. According to previous research on the solidification characteristics of Al_2O_3-reinforced Al-MMCs, the primary α phase is efficient in rejecting the Al_2O_3 and pushing the particles ahead of the solid/liquid interface. In this regard, a critical solid/liquid interface velocity has been reported, above which the Al_2O_3 particles are engulfed by the moving interface and below which they

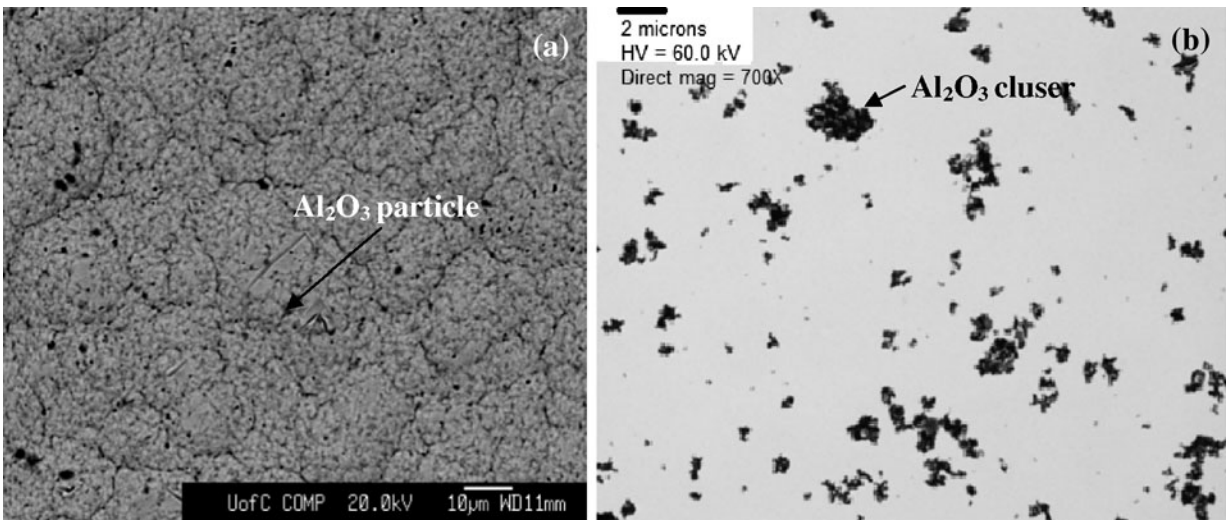

Fig. 3—(*a*) Surface of the Ni-Al_2O_3 coating produced by electrodeposition. (*b*) TEM image of the nanosized Al_2O_3 powder prior to deposition.

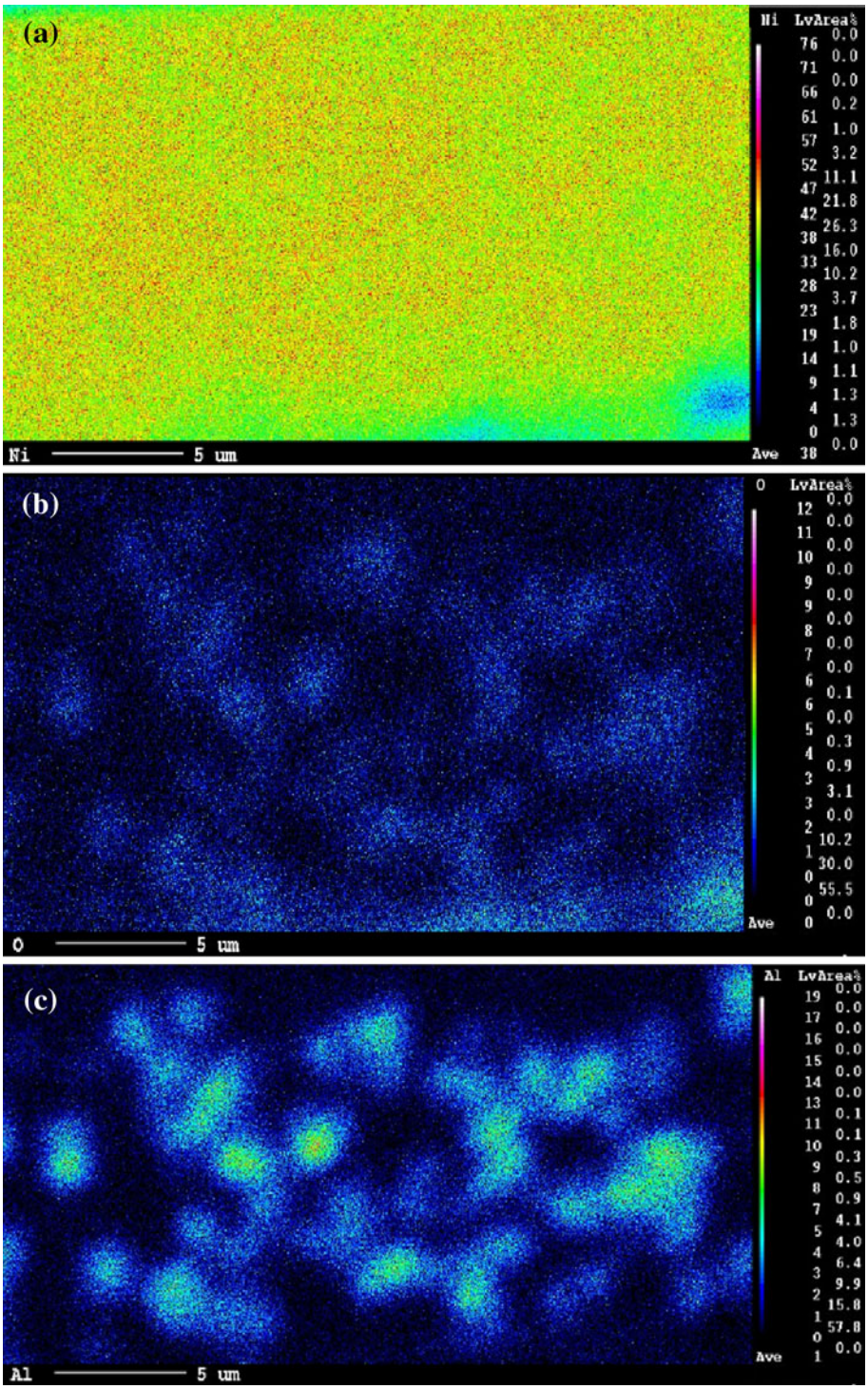

Fig. 4—X-ray digital composition maps taken from the Ni-Al_2O_3 coating surface for (*a*) Ni, (*b*) O, and (*c*) Al.

are pushed toward the joint center.[19,20] Cooke *et al.*[13–15] proposed Eq. [3] for predicting the width of the segregated zone that forms during the solidification stage of TLP bonding of Al-MMCs when a nanocomposite coating is used as the interlayer.

$$S_{SZ} = W_{max}\left(\frac{\delta_p + \chi_2}{\delta_p + \chi_1}\right) \quad [3]$$

where δ_p is the diameter of the particles in the as received material, χ_1 is the interparticle spacing in the as-received material, and χ_2 is the interparticle spacing after bonding. By assuming $\delta_p = 28\ \mu m$, $\chi_1 = 10\ \mu m$, and $\chi_2 = 0$, Cooke *et al.*[15] found that the width of the segregated zone is approximately 74 pct of the width of the maximum liquid phase that forms during bonding. This can be written as $S_{sz} = 0.74 W_{max}$. Additionally,

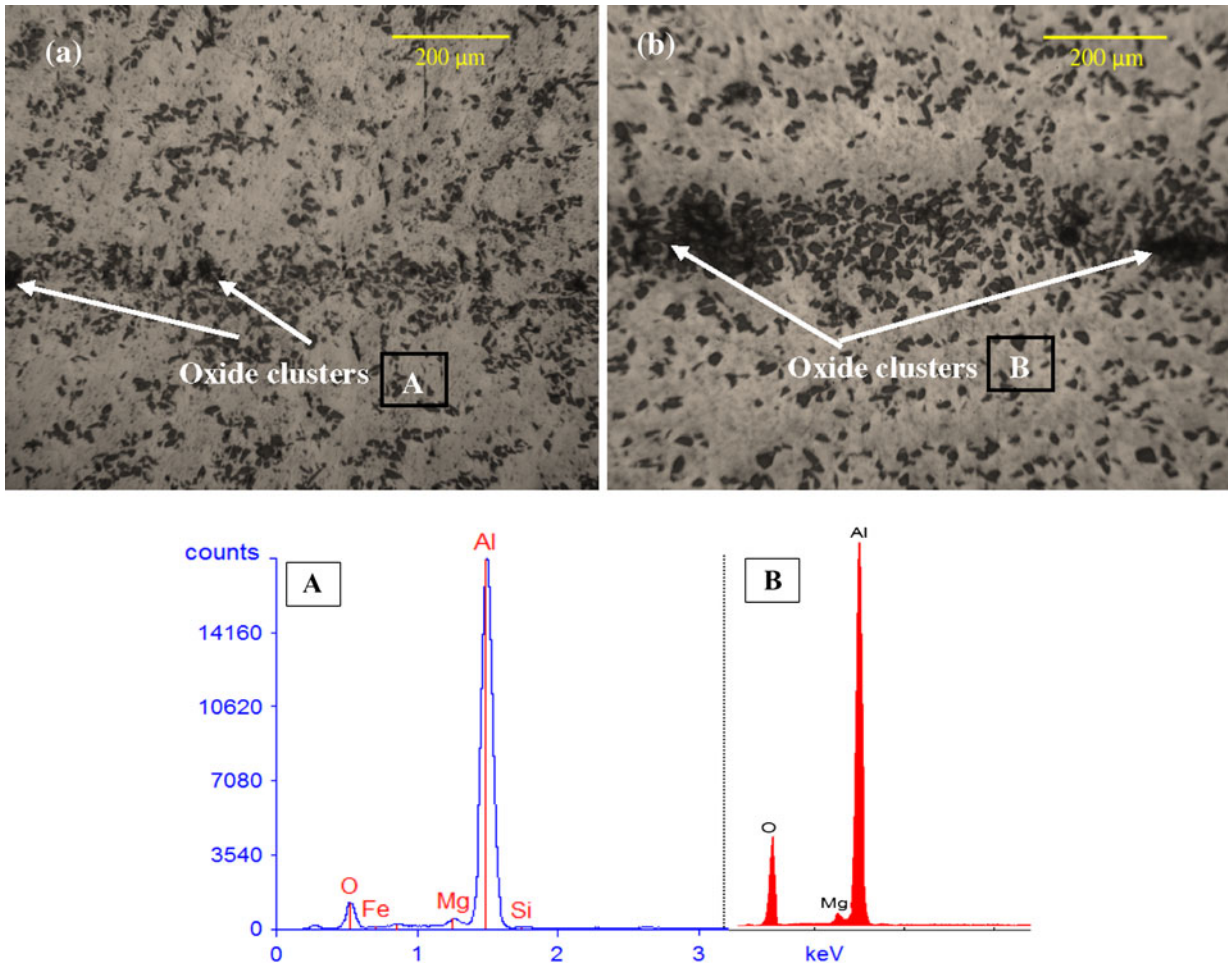

Fig. 5—Microstructure of joints bonded at 873 K (600 °C) for 10 min using (*a*) 5-μm thick Ni-(500 nm) Al_2O_3 and (*b*) 5-μm thick Ni-(50 nm) Al_2O_3. EDS analyses of the clusters are shown in (A) and (B), respectively.

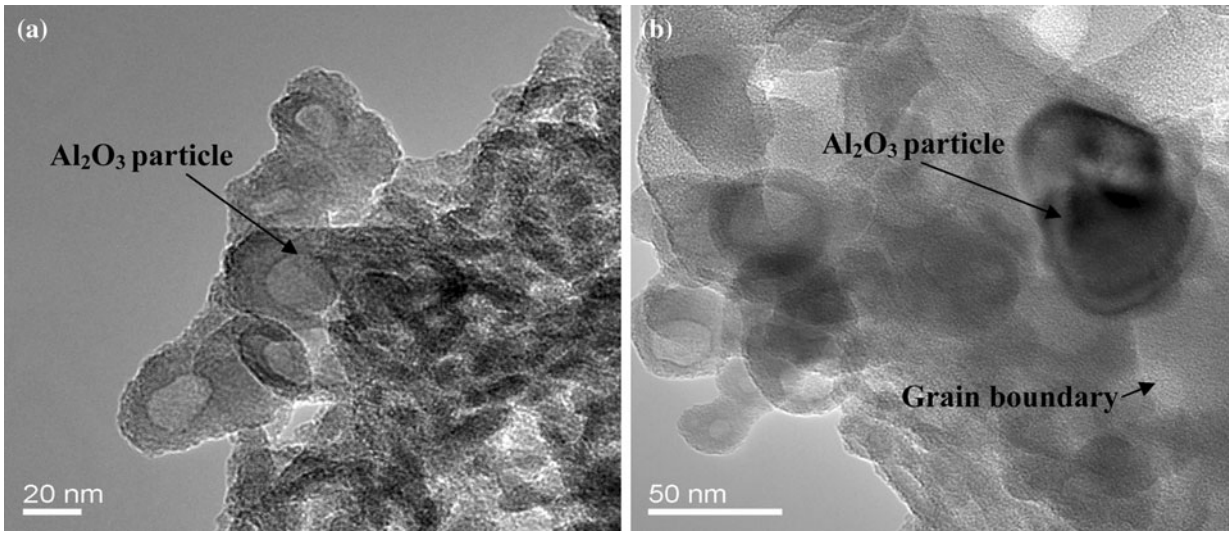

Fig. 6—(*a*) TEM image of the bonded joint when nanosized Al_2O_3 particles are used in the interlayer and (*b*) TEM image of a nano-Al_2O_3 particle located at a grain boundary.

the authors showed that the relationship between the initial width of the interlayer and the maximum liquid width can be $W_{max} = 20.6w_o$. By substituting this relationship into Eq. [3], it was shown that $S_{SZ} = 0.74(20.6w_o) = 15.2w_o$, which suggests that the width of the segregated zone is approximately 15 times

the thickness of the interlayer at the start of the bonding process.

However, because the initial interlayer width was held constant for all samples bonded, the width of the segregated zone should have been similar. The hypothesis is that the difference in the width of the segregated zone obtained is dependent on the differences in the particle size and the distribution of the nanosized particles in the joint zone during bonding. TEM analyses indicated that the nanoparticles are arranged along the grain boundary as shown in Figure 6, which would impart a pinning effect as described by Orowan.[21]

WDS analyses of the joints as a function of the particle size indicated that the Ni concentration was 0.95 wt pct and 0.79 wt pct for samples bonded using 500 nm and 50 nm, respectively. The lower concentration obtained when 50 nm particles are used suggest a faster diffusivity of Ni during the bonding process. This finding was attributed to greater surface contact between the uncoated Al-6061 sample and the Ni-Al_2O_3 coating surface. An analysis of the roughness using SEM indicated that the surface roughness increased from 0.1 μm for coatings containing 50-nm particles to 0.25 μm for a coating containing 500-nm particles.

C. *Microhardness Measurements*

The degree of compositional homogeneity achieved across the joint region was assessed by microhardness testing. A uniform hardness across the joint would indicate good chemical homogeneity and particle distribution. The hardness profiles for the joints made as a function of the interlayer particle size are shown in Figure 7. The results indicated that the hardness value within the joint zone increased with the decreasing particle size from 122 VHN at 500 nm to 132 VHN at 50 nm. In all profiles shown, the highest hardness value was recorded at the joint center, and it decreased with increasing distance from the joint center into the base metal. The fluctuation in hardness value within joint zone was attributed to the random distribution of ceramic particles within the soft aluminum matrix. The scientific literature suggests that the geometrical constraints from the Orowan strengthening mechanism can result in an increase in the hardness when the particle size is reduced.[22]

An XRD analysis of the polished cross section of a bonded made at a bonding temperature of 873 K (600 °C) shown in Figure 8 revealed strong peaks for Al_2O_3 and intermetallics compounds such as Al_3Ni, Ni_3Si, and Al_9FeNi. These compounds can also contribute to the high hardness number recorded in the joint region.

D. *Shear Strength Measurements*

Figure 9 shows the joint shear strength profile as a function of the interlayer particle size. The result indicated that the joint shear strength increased with the decreasing particle size from 138 MPa (standard deviation of 2.01) with 500 nm to 142 MPa (standard deviation of 3) with 50 nm; however, when pure nickel coating was used, a joint strength of only 117 MPa was obtained. The increase in joint shear strength was attributed to a uniform distribution of the 50-nm particles within the joint zone. The results indicated that joint strength of up to 92 pct of the base metal strength (154 MPa) is achievable when using a 50-nm diameter, nanosized, particle-reinforced interlayer. Tjong[22] showed that the nanoparticle size has a strong

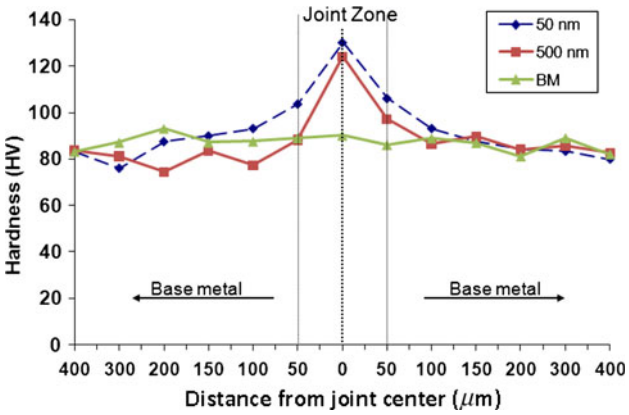

Fig. 7—Microhardness profiles of the hardness variation across the bond interface as a function of the particle size.

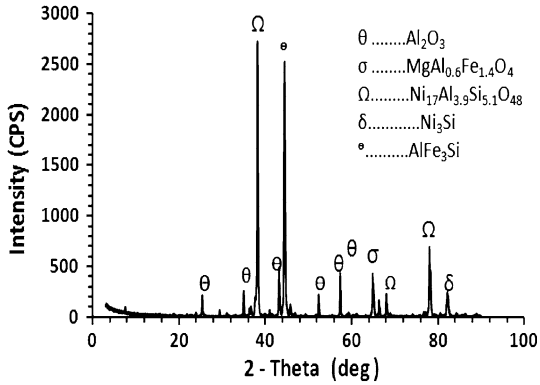

Fig. 8—XRD analysis of the polished surface for a bond made with 5-μm thick Ni-(50 nm) Al_2O_3 for 10 min at 873 K (600 °C).

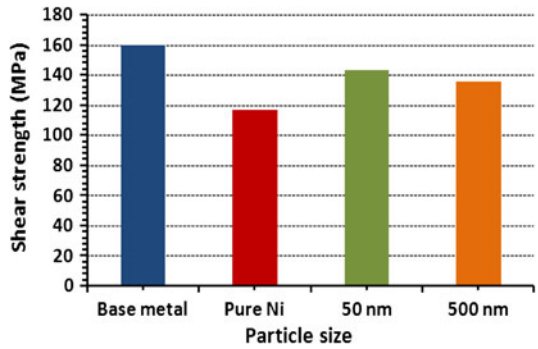

Fig. 9—Joint shear strengths as a function of particle size using 5-μm-thick coatings.

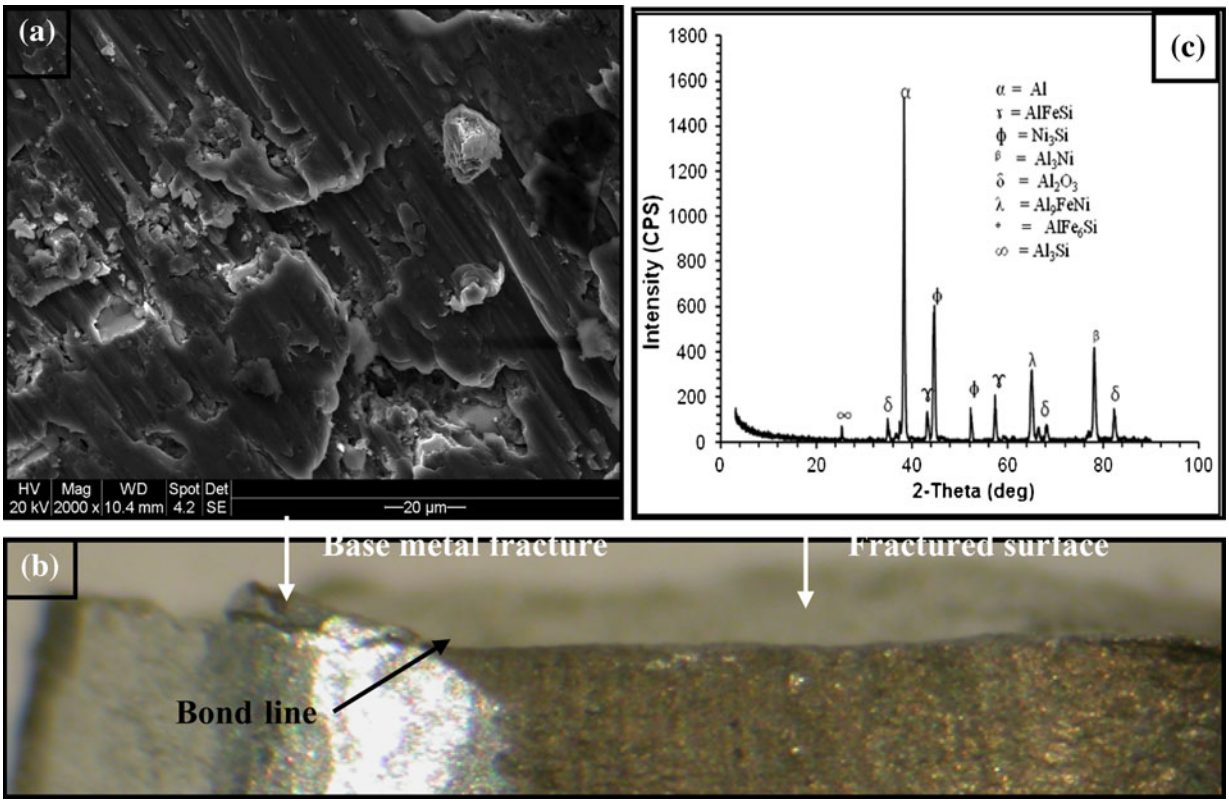

Fig. 10—(*a*) SEM micrograph, (*b*) cross section, and (*c*) XRD analysis of the fractured surface for a bond made with 5-μm-thick Ni-(500 nm) Al_2O_3 for 10 min at 873 K (600 °C).

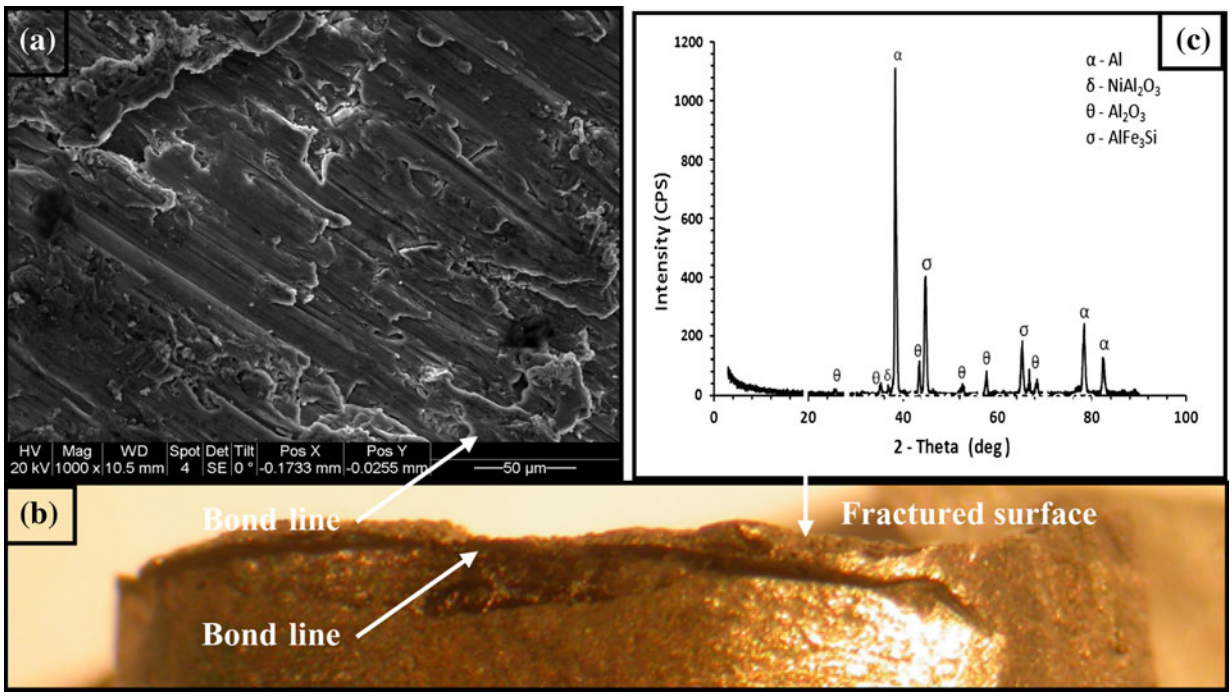

Fig. 11—(*a*) SEM micrograph, (*b*) cross section, and (*c*) XRD analysis of the fractured surface for a bond made with 5-μm-thick Ni-(50 nm) Al_2O_3 for 10 min at 873 K (600 °C).

effect on the yield strength. The author suggested that a particle size of 100 nm is a critical value for improving the yield strength of nanocomposites. Below this critical value the yield strength increases significantly with decreasing particle size. When the particle size was increased to 500 nm, the joint strength decreased from 142 MPa when 50-nm particles were used to 138 MPa. Similar results were obtained by Gupta and coworkers.[23,24] Zhang and Chen[21] showed that the Orowan stress plays a major role in strengthening the nanocomposites.

A fractographic analysis of the fractured surface for a bond made using the 500-nm Al_2O_3 particle in the interlayer is shown in Figure 10. The fractured surface showed evidence of shear plastic deformation, indicative of ductile fracture with a crack propagating through the bond line and a section of the base metal adjacent to the bond line (Figure 10(b)). A similar result was obtained when the 50-nm particles were used in the coating (Figure 11). The results show that in both cases, sufficient liquid was formed at the interface during the bonding process and could remove all the surface oxide present, resulting in metal-to-metal contact. XRD analyses of the fractured surfaces indicated the presence of peaks for Al_2O_3, $NiAl_2O_4$, and $Al_{11}Ni_9$ compound at the fractured surface.

IV. CONCLUSIONS

The results of the study indicated that Al 6061 metal–matrix composite containing 15 vol pct Al_2O_3 particles can be bonded successfully using transient liquid phase diffusion bonding with the aid of Ni-coating containing a dispersion of nano-Al_2O_3. The joint structure described was attributed to the formation of a ternary Al-Ni-Si eutectic liquid. The highest joint strength of 142 MPa was achieved for bonds made using 50-nm Al_2O_3 particles in the interlayer. The results indicated that particle segregation along the bond interface has a detrimental effect on the strength of the joint produced. The formation of particle-rich region within the joint zone leads to the development of stress concentration points, which decreases the joint strength. However, the joint strength of approximately 92 pct of the base metal strength is achievable when the Ni/Al_2O_3 nanocomposite is used as the interlayer.

ACKNOWLEDGMENT

The authors thank Mr. Charles Rau of Technologies Green Partners, San Diego, CA for providing the test material.

REFERENCES

1. M.B.D. Ellis: *TWI J.*, 1997, vol. 6, pp. 69–128.
2. T. Pal Kumar: *J. Mater. Manufact. Process.*, 2005, vol. 20, pp. 717–26.
3. G. Zhang, J. Zhang, Y. Pei, S. Li, and D. Chai: *Mater. Sci. Eng. A*, 2008, vol. 488 (1–2), pp. 146–56.
4. W.D. Macdonald and T.W. Eager: *Miner. Metal. Join. Soc.*, 1992, pp. 93–101.
5. I. Tuah-Poku, M. Dollar, and T.B. Massalski: *Metall. Trans. A*, 1988, vol. 19A, pp. 675–86.
6. Y. Zhou, W.F. Gale, and T.H. North: *Phase Bonding, Int. Mater. Rev.*, 1995, vol. 40 (5), pp. 181–96.
7. J. Huang, Y. Dong, J. Zhang, Y. Wan, and G. Zhou: *J. Mater. Sci. Technol.*, 2005, vol. 21 (5), pp. 779–81.
8. Z. Li, Y. Zhou, and T.H. North: *Mater. Sci.*, 1995, vol. 30, pp. 1075–82.
9. X.L. Zhong and M. Gupta: *Adv. Eng. Mater.*, 2005, vol. 7 (11), p. 1049.
10. S. Weis, I. Hoyer, and B. Wielage: *Weld J.*, 2008, vol. 86, pp. 35–37.
11. B. Wielage, I. Hoyer, and S. Weis: *Weld J.*, 2007, vol. 86, pp. 67–70.
12. J. Yan, Z. Xu, S. Lei, X. Ma, and S. Yang: *Mater. Des.*, 2011, vol. 32, pp. 343–47.
13. K. Cooke, T. Khan, and G. Oliver: *Metall. Mater. Trans. A*, 2011, vol. 42A, pp. 1271–77.
14. K. Cooke, T. Khan, and G. Oliver: *Mater. Design*, 2012, vol. 33, pp. 469–75.
15. K.O. Cooke, T.I. Khan, and G.D. Oliver: *Weld J.*, 2012, vol. 17 (1), pp. 22–31.
16. J.K. Dennis and T.E. Such: *Nickel and Chromium Plating*, 3rd ed., ASM International, Materials Park, OH, 1993.
17. E. Dmitry, G. Belov, N.A. Aksenov, and A. Andrey: *Multicomponent Phase Diagrams: Applications for Commercial Aluminum*, Elsevier, Atlanta, GA, 2005.
18. ASTM E3-01, Standard Preparation for Metallographic Examination, 2008.
19. D.M. Stefanescu, F.R. Juretzko, B.K. Dhindaw, A. Catalina, S. Sen, and P.A. Curreri: *Metall. Mater. Trans. A*, 1998, vol. 29A, pp. 1697–706.
20. S. Mukherjee and D.M. Stefanescu: *Metall. Mater. Trans. A*, 2004, vol. 35A, pp. 613–21.
21. Z. Zhang and D.L. Chen: *Scripta Mater.*, 2006, vol. 54, p. 1321.
22. S.C. Tjong: *Adv. Eng. Mater.*, 2007, vol. 9 (8), p. 511.
23. S.F. Hassan and M. Gupta: *J. Mater. Sci. Technol.*, 2004, vol. 20, p. 1383.
24. N. Srikanth, S.F. Hassan, and M. Gupta: *J. Compos. Mater.*, 2004, vol. 38, p. 2037.